This is an open access article published under an ACS AuthorChoice License, which permits copying and redistribution of the article or any adaptations for non-commercial purposes.

JACS
JOURNAL OF THE AMERICAN CHEMICAL SOCIETY
Article
pubs.acs.org/JACS

Squaraine-Based Polymer Dots with Narrow, Bright Near-Infrared Fluorescence for Biological Applications

I-Che Wu,[†,‡] Jiangbo Yu,[†,‡] Fangmao Ye,[†] Yu Rong,[†] Maria Elena Gallina,[†] Bryant S. Fujimoto,[†] Yong Zhang,[†] Yang-Hsiang Chan,[†,∥] Wei Sun,[†] Xing-Hua Zhou,[†] Changfeng Wu,[§] and Daniel T. Chiu*[,†]

[†]Department of Chemistry, University of Washington, Seattle, Washington 98195, United States

[§]State Key Laboratory on Integrated Optoelectronics, College of Electronic Science and Engineering, Jilin University, Changchun 130012, China

Supporting Information

ABSTRACT: This article describes the design and development of squaraine-based semiconducting polymer dots (Pdots) that show large Stokes shifts and narrow-band emissions in the near-infrared (NIR) region. Fluorescent copolymers containing fluorene and squaraine units were synthesized and used as precursors for preparing the Pdots, where exciton diffusion and likely through-bond energy transfer led to highly bright and narrow-band NIR emissions. The resulting Pdots exhibit the emission full width at half-maximum of ∼36 nm, which is ∼2 times narrower than those of inorganic quantum dots in the same wavelength region (∼66 nm for Qdot705). The squaraine-based Pdots show a high fluorescence quantum yield (QY) of 0.30 and a large Stokes shift of ∼340 nm. Single-particle analysis indicates that the average per-particle brightness of the Pdots is ∼6 times higher than that of Qdot705. We demonstrate bioconjugation of the squaraine Pdots and employ the Pdot bioconjugates in flow cytometry and cellular imaging applications. Our results suggest that the narrow bandwidth, high QY, and large Stokes shift are promising for multiplexed biological detections.

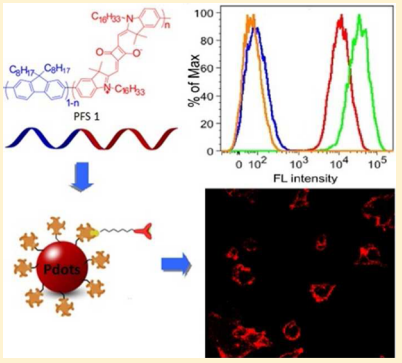

INTRODUCTION

Near-infrared (NIR) fluorescent probes have been widely used in biological and biomedical research because light in this wavelength region has a large penetration depth in tissue and causes minimal cellular autofluorescence.[1] Organic dyes are the most commonly used NIR fluorescent probes, despite their non-optimal brightness and photostability. They are extensively used in fluorescence imaging and assays because of their well-established labeling protocols and their molecular dimensions.[2−8] However, the use of organic NIR probes for bioimaging applications encounters several difficulties. For example, organic NIR dyes usually consist of large, hydrophobic conjugated systems that may lead to aggregation in physiological environments, which can dramatically reduce their emission quantum yield (QY) and broaden their emission spectra as compared with dyes emitting in the visible range.[9] In addition, the Stokes shifts for organic NIR dyes are generally very small, which is not optimal for imaging applications because cross-talk between the excitation light and fluorescence can make it difficult to capture the pertinent signals.[9] In the past decade, inorganic semiconductor quantum dots (Qdots) were developed as NIR probes because they offer significantly higher photostability and brightness compared to conventional dyes.[10−12] The potential leakage of heavy metal ions from the Qdots and the subsequent cell toxicity, however, are critical concerns for biological applications.[12−15]

Semiconducting polymer dots (Pdots) with small sizes (<30 nm) are a new class of highly fluorescent probes that possess extraordinary brightness, fast emission rates, good photostability, and minimal toxicity to biological cells and tissues.[16−22] There are recent efforts in developing Pdots with NIR emission as fluorescent probes.[23−25] One strategy is based on encapsulation of a hydrophobic NIR dye in Pdots with visible emission.[23,24] Upon light excitation, the Pdots transfer the energy efficiently to the dopant dye, resulting in quenching of visible emission with concomitant NIR emission. However, this dye-doping approach can have a dye leakage problem in applications that occur over relatively long periods of time and during storage.[20,23,25] Another method is to blend a NIR-emitting polymer as an acceptor with several semiconducting polymers such as red, green, and blue-emitting polymers as donors that work together via cascade fluorescence resonance energy transfer (FRET) to generate NIR-emitting Pdots.[25] The design and synthesis of these polymers for cascade FRET are relatively complicated, and much work must be done to optimize the blending ratios of the semiconducting polymers to get high fluorescence QY and efficient energy transfer.

Many biological applications require that the fluorescent probes possess narrow-band emissions for multiplexed detections. For example, in a wavelength-and-intensity multiplexing scheme for optical encoding, the number of codes increases greatly with increasing number of color and intensity levels. Previous studies suggest that it is better to use more colors, rather

Received: July 23, 2014
Published: December 10, 2014

 © 2014 American Chemical Society dx.doi.org/10.1021/ja5123045 | J. Am. Chem. Soc. 2015, 137, 173−178

than more intensity levels, in order to increase the number of usable codes.[26] Therefore, development of narrow, bright NIR Pdots remains an important task for widespread biological applications. This article describes the design and synthesis of squaraine-based Pdots that show large Stokes shifts and narrow-band emissions in the NIR region. The squaraine Pdots exhibit an emission bandwidth of ~36 nm (full width at half-maximum, fwhm), about 2 times narrower than those of Qdots in the same wavelength region. To our knowledge, this is the narrowest emission bandwidth among various Pdot species reported so far. The narrow bandwidth, high QY, and large Stokes shifts of the squaraine-based Pdots are promising for multiplexed biological detections.

RESULTS AND DISCUSSION

Scheme 1 shows the chemical structures of the squaraine-based polymers (PFS1 and PFS2) and the scheme for forming Pdot bioconjugates. The squaraine units were chosen because of their strong absorption and narrow emission band centered in the NIR region (700–720 nm). Two types of squaraine-based units were synthesized and incorporated into the polyfluorene backbone with different squaraine–fluorene ratios (squaraine monomer for polymer PFS1 and benzene fused squaraine monomer for polymer PFS2). The detailed synthesis procedure of the squaraine monomer and polymer PFS1 is included in Schemes S1 and S2 (Supporting Information). To further shift the emission peak to the NIR, a benzene ring fused squaraine monomer was also designed and prepared for polymer synthesis. Benzene fused squaraine shows increased conjugation length that generally produces a red-shifted emission. The synthesis procedure for this fused squaraine monomer and polymer PFS2 is shown in Scheme S3 and S4 (Supporting Information).

Scheme 1. Chemical Structures of PFS1, PFS2, and PS-PEG-COOH Polymers[a]

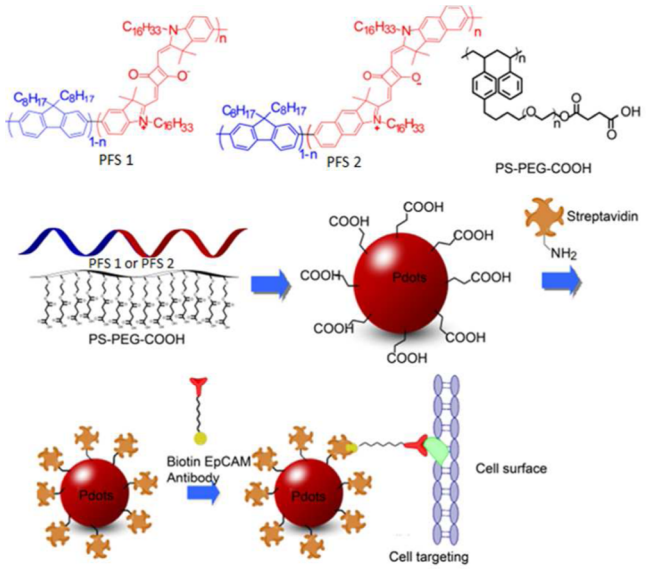

[a]The schematic depicts the process of Pdot preparation, bioconjugation, and cellular labeling.

Optimization of Monomer Ratio and Polymer Composition. We systematically studied the optical properties of the Pdots as we varied the monomer ratios, as squaraine concentration greatly affects the emission spectra and QY of the Pdots. From the fluorescence spectra (Figure 1), all the copolymers in THF solutions show two emission peaks, around 420 and 700 nm, respectively. The former originates from the polyfluorene backbone and the latter is from the squaraine derivatives. The intensity ratio (R) of the NIR emission peak to the blue emission peak increases with increasing feeding ratios of squaraine (Table S1). When these polymers were prepared into Pdots, the nanoparticles in aqueous solution showed similar trend in spectral evolution with dramatically increased NIR emissions relative to the blue emission. However, the QY of the NIR emission were also dramatically decreased with the higher feeding ratio of squaraine monomers.

When the Pdots were excited with 405 nm light, we observed strong NIR emission, despite the fact that there was almost no spectral overlap (Figure 2) between the emission of the energy donor (polyfluorene) and the absorption of the acceptor/emitter (squaraine monomer). Energy transfer between molecules without significant spectral overlap has been reported.[27,28] We believe the mechanism for the efficient energy transfer from polyfluorene to squaraine likely is not based on FRET. Rather, energy transfer likely occurred first through exciton diffusion along the fluorene polymer backbone[29−31] followed by through-bond energy transfer[27,28] to the squaraine monomer.

Fluorescence lifetime measurements (Figure 2c,d) are helpful for clarifying the mechanism of energy transfer processes. We measured the fluorescence lifetimes of different donors and acceptors in blended squaraine Sq1/PFO and PFS1 Pdots (Figure 2c). From the fitted lifetime decay curves, the lifetime values were 0.27 and 0.08 ns for fluorene in blended squaraine Sq1/PFO Pdots and in PFS1 Pdots, respectively; for squaraine in blended squaraine Sq1/PFO Pdots and in PFS1 Pdots, the values were 2.0 and 2.24 ns, respectively. These values indicate fluorenes in PFS1 Pdots have a significantly shorter fluorescence lifetime than those in the blended squaraine Sq1/PFO Pdots, which is comparable to the published values for PFO Pdots. This result suggests energy transfer from the fluorene donor to the squaraine acceptor in PFS1 Pdots was much more efficient than that in the blended Pdots; the enhanced intraparticle energy transfer is the dominant factor that made PFS1 Pdots strong NIR emitters. Similarly, in PFS2 Pdots, the luminescence lifetime of fluorene donor was also shortened to 0.08 ns, which indicates there was also an enhanced energy transfer in these Pdots. In PFS2 Pdots, the NIR emission from the fused squaraine acceptor also had a longer lifetime of 2.12 ns.

Table S1 summarizes the photophysical properties of the two sets of Pdots with different monomer ratios. It is clear that the fluorescence QY decreased with increased squaraine concentrations. For example, the QY of PFS1 Pdots decreased from 30% to 2% when the molar ratio of the squaraine chromophore was increased from 1.5% to 10%. Similarly, the PFS2 Pdots exhibited a decrease in QY from 17% to 1% as the molar content of benzene-fused squaraine increased from 1.5% to 10%. We attribute this phenomenon to aggregation of the squaraine chromophores in Pdots, consistent with the slight red-shift observed in the Pdot fluorescence spectra. From these experiments, we determined that Pdots consisting of 1.5% squaraine offered the best overall performance in terms of the emission bandwidth and brightness.

Colloidal and Photophysical Properties of Optimized Pdots. Figure 3 shows the spectroscopic and colloidal properties for the final optimized form of the two types of Pdots. An average diameter of 18 nm was determined for both Pdots by dynamic light scattering (DLS, Figure 3e,f), and further confirmed by

dx.doi.org/10.1021/ja5123045 | J. Am. Chem. Soc. 2015, 137, 173−178

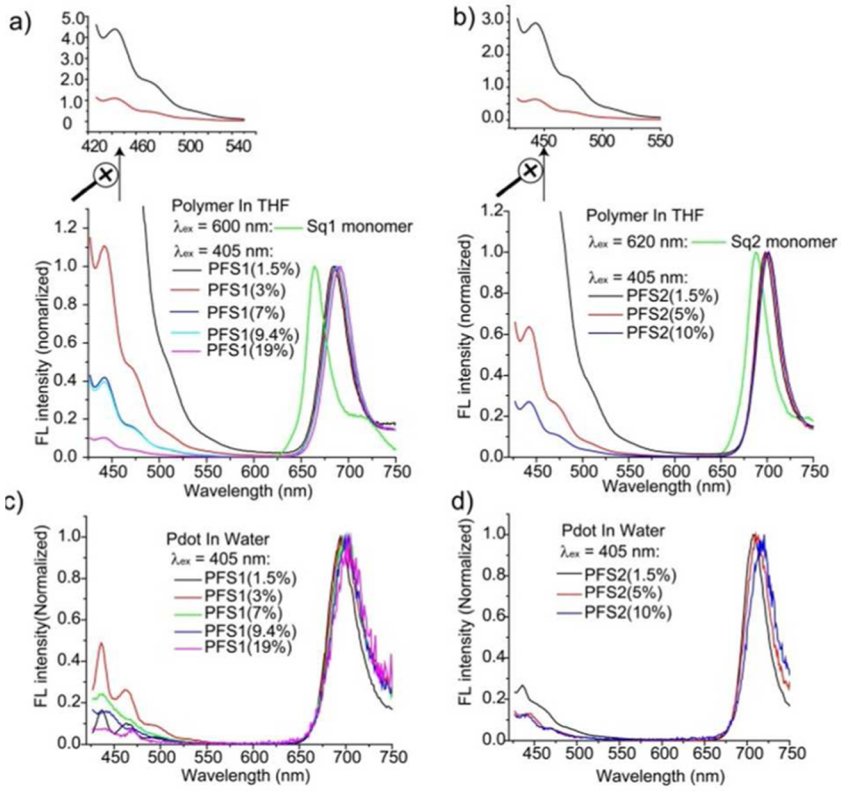

Figure 1. (a) Emission spectrum for squaraine monomer (Sq1) in THF (λ_{ex} = 600 nm, green), and emission spectra of PFS1 polymers in THF solution with different molar ratios of acceptor squaraine (λ_{ex} = 405 nm): 1.5% (black), 3% (red), 7% (blue), 9.4% (cyan), and 19% (magenta). The inset shows the enlarged region of the fluorescence spectra of 1.5% (black) and 3% (red) PFS1 polymers in the range of 420−550 nm. (b) Emission spectrum for fused squaraine monomer (Sq2) in THF (λ_{ex} = 620 nm, green), and emission spectra of PFS2 polymers in THF solution with different molar ratios of acceptor fused squaraine (λ_{ex} = 405 nm): 1.5% (black), 5% (red), and 10% (blue). The inset shows the enlarged region of the fluorescence spectra of 1.5% (black) and 5% (red) PFS2 polymers in the range of 420−550 nm. (c) Emission spectra of different PFS1 Pdots made from the above PFS1 polymers in H_2O (λ_{ex} = 405 nm): 1.5% (black), 3% (red), 7% (green), 9.4% (blue), and 19% (magenta) of acceptor squaraine. (d) Emission spectra of different PFS2 Pdots made from the above PFS2 polymers in H_2O (λ_{ex} = 405 nm): 1.5% (black), 5% (red), and 10% (blue) of fused squaraine acceptors.

transmission electron microscopy (TEM, Figure 3c,d). From the absorption spectra, both Pdots showed strong absorption peaks around 375 nm due to the polyfluorene backbone. The fluorescence spectra show strong emission centers at 693 nm for PFS1 Pdots, and 711 nm for PFS2 Pdots. Both Pdots show large Stokes shifts of over 320 nm and exhibit narrow emission bandwidths (fwhm ~36 nm), which is comparable to or narrower than most NIR organic dyes, and about 2 time narrower than that of Qdots emitting in similar wavelength region (~66 nm for commercially available Qdot705). Because the emission spectra of Pdots show a tail at longer wavelengths, we also compared the full width at 10% of maximal intensity between PFS1 Pdot and Qdot705 (Figure S1); here, Pdot is still ~37 nm narrower than Qdot. The narrow emission bandwidth is important for preventing emission cross-talk among probes, particularly for multicolor labeling and multiplexed biological detections.

Single-Particle Brightness Comparison. For using Pdots as fluorescent labels, the final brightness of Pdots can be estimated by the product of the peak absorption cross-section and the fluorescence QY of the NIR emission of the Pdots. The absorption cross-section is the light-harvesting capability of a fluorescent probe at a given wavelength, which can be determined from the absorption spectra. An analysis of the UV−vis spectra at known PFS1 and PFS2 Pdot concentrations shows the per-particle absorption cross sections of the Pdots (18 nm in diameter) at 405 nm were 2.4×10^{-13} cm^2 for PFS1 Pdots and 1.9×10^{-13} cm^2 for PFS2 Pdots, which are close to the reported values of other types of Pdots.[16,18,32] We performed single-particle imaging to experimentally compare the single-particle brightness between Qdot705 and the Pdots under identical excitation and collection conditions. The PFS1 Pdots, PFS2 Pdots, and Qdot705 were excited with a 405 nm laser, and a long-pass filter of 685 nm was used. Figure 4 shows the single-particle images of the three nanoparticles; intensity histograms were obtained by analyzing hundreds of nanoparticles from each sample. We found PFS1 Pdots were about six times brighter than Qdot705 and PFS2 Pdots were about three times brighter than Qdot705, consistent with their measured photophyiscal parameters.

Cellular Labeling, Flow Cytometry, and Fluorescence Imaging. To use the NIR-emitting Pdots for biological labeling and targeting, we functionalized the Pdot surface with carboxyl groups and carried out bioconjugation with streptavidin using EDC-catalyzed coupling as described in our previous reports (Scheme 1).[18−20,25,32] Pdot-streptavidin (Pdot-SA) was used to label cell-surface markers on MCF-7 breast cancer cells. The cells were sequentially incubated with biotinylated primary anti-EpCAM antibody and Pdot-SA probes. Flow cytometry was performed to examine the specificity and brightness of labeling by the Pdot-streptavidin probes (Figure 5). The labeled cells exhibited stronger fluorescence compared with the control samples, indicating the two Pdots effectively and specifically

dx.doi.org/10.1021/ja5123045 | J. Am. Chem. Soc. 2015, 137, 173−178

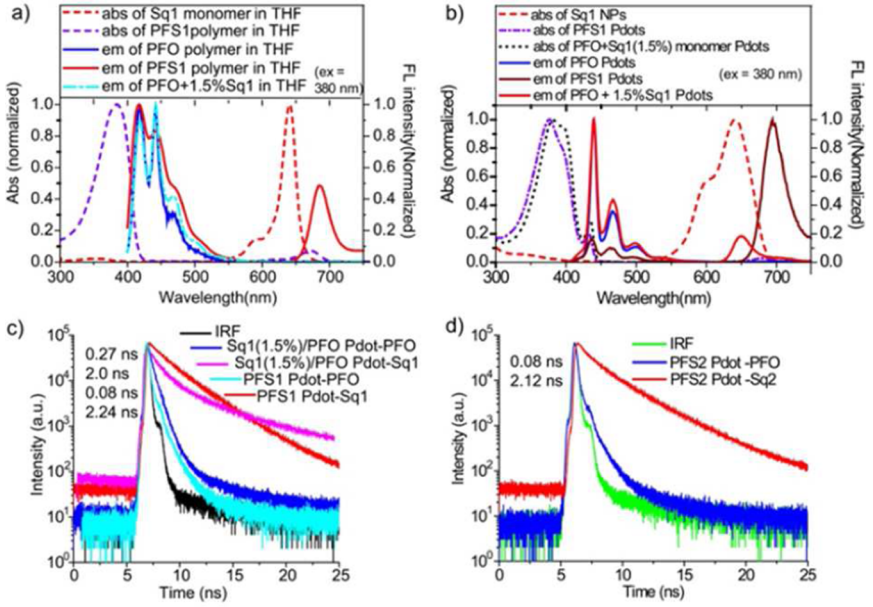

Figure 2. (a) Absorption spectra of squaraine monomer (Sq1) in THF (red dash) and PFS1 polymer in THF (violet dash), and emission spectra of PFO polymer in THF (blue solid), PFS1 polymer in THF (red solid), and PFO polymer mixed with 1.5% (in molar ratio) Sq1 monomer in THF (cyan dash-dot). (b) Absorption spectra of Sq1 monomer doped in amphiphilic PS-PEG-COOH (20 wt%) polymer nanoparticle in H_2O (red dash), PFS1 Pdots in H_2O (violet dash-dot), and PFO polymer blended with 1.5% (in molar) Sq1 monomer Pdots in H_2O (black dot), and emission spectra of PFO Pdots in H_2O (blue solid), PFS1 Pdots in H_2O (burgundy solid), and blended Pdots prepared from PFO polymer mixed with 1.5% (in molar ratio) Sq1 monomer (red solid). (c) Instrument response function (IRF) curve (black), lifetime decay curves of the fluorescence from blended Sq1/PFO Pdots in H_2O, which include the lifetime decay for the fluorescence from fluorene groups of PFO polymer in Pdots (blue) and from squaraine monomer Sq1 in Pdots (magenta), and lifetime decay curves of the fluorescence from PFS1 Pdots in H_2O, which include the lifetime decay for the fluorescence from fluorene groups in PFS1 Pdots (cyan) and from squaraine groups in PFS1 Pdots (red). (d) Lifetime decay curves of the fluorescence from fluorene groups in PFS2 Pdots in H_2O (blue) and from squaraine groups in PFS2 Pdots in H_2O (red). All emission spectra were obtained at an excitation of λ_{ex} = 380 nm. All fluorescence lifetime measurements were obtained at an excitation from a laser tuned to λ_{ex} = 375 nm.

Table 1

sample	size (nm)	λ_{em} (nm)	σ^b ($\times 10^{-13}$ cm^2)	QY^c (%)	fwhm (nm)	τ^d (ns)
Qdot705	13	705	0.32	41	66	65[33]
PFS1	18[a]	693	2.4	30	36	2.24
PFS2	18[a]	711	1.9	17	36	2.12

[a]Average size measured by DLS. [b]Single-particle absorption cross-section at 405 nm. [c]Quantum yield was measured at a 405 nm excitation wavelength. [d]Fluorescence lifetime.

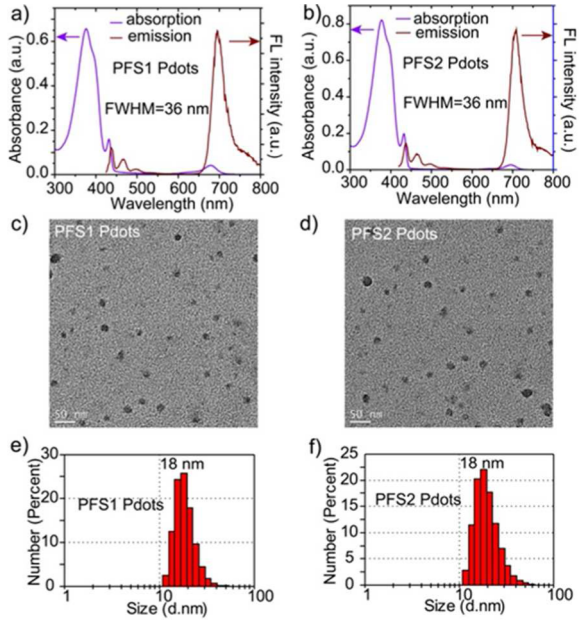

Figure 3. Absorption and emission spectra (λ_{ex} = 380 nm) of (a) PFS1 and (b) PFS2 Pdots in water. TEM images for (c) PFS1 Pdots and (d) PFS2 Pdots; scale bar is 50 nm. Histograms of size distribution measured by DLS for (e) PFS1 Pdots and (f) PFS2 Pdots; both show an average diameter of 18 nm.

labeled EpCAM receptors on the cell surface with excellent brightness. The negative control samples were prepared under identical conditions as the positive ones but without primary biotinylated antibodies. We compared the PFS1 and PFS2 Pdots-SA with commercial Qdot705-SA under the same labeling concentrations and identical experimental conditions (Figure 5). The results indicate PFS1-SA and PFS2-SA Pdots were about six and three times brighter than that of Qdot705-SA, respectively, which are consistent with the single-particle brightness measurements shown in Figure 4. From the negative control samples, it can be seen that both Pdot probes also exhibited less non-specific binding to cells than the Qdot probe.

We further confirmed specific cellular labeling with PFS1 Pdot-SA and PFS2 Pdot-SA probes by confocal fluorescence imaging (Figure 6). These results also show PFS1 (Figure 6a) and PFS2 Pdot-SA (Figure 6b) probes effectively and specifically labeled EpCAM receptors on the MCF-7 cell surface; in the equivalent negative control experiments (data not shown) where the primary biotinylated antibody was absent, no fluorescence was detected, again indicating little or no non-specific binding of the Pdots to the cells.

dx.doi.org/10.1021/ja5123045 | J. Am. Chem. Soc. 2015, 137, 173−178

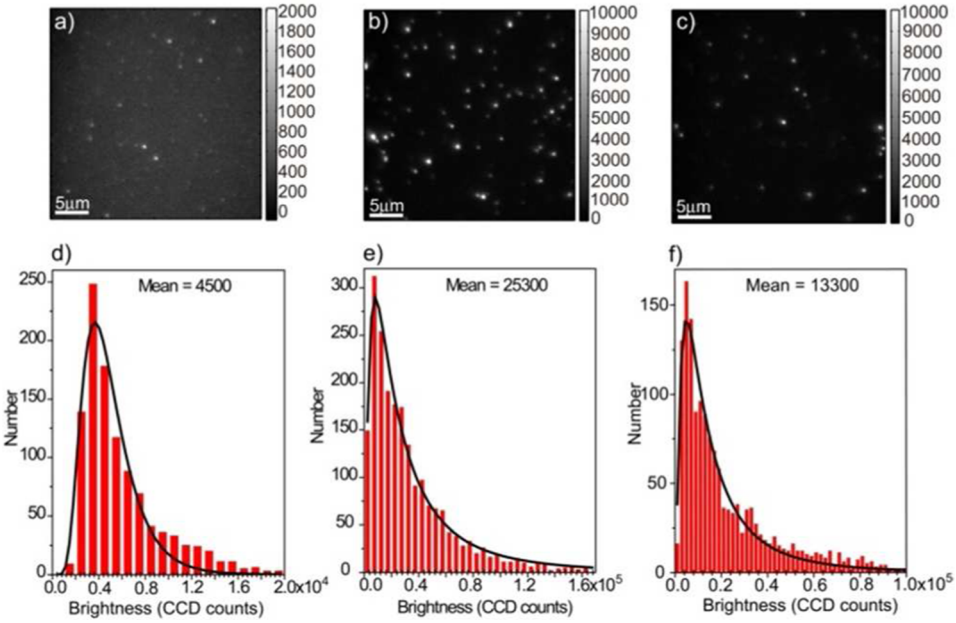

Figure 4. Single-particle fluorescence images of (a) Qdot705, (b) PFS1 Pdots, and (c) PFS2 Pdots obtained with a 405 nm laser using the same excitation power and under identical detection conditions. Histograms of the distributions of single-particle brightness of (d) Qdots705, (e) PFS1 Pdots, and (f) PFS2 Pdots. The black curves were obtained by fitting a log-normal function to the histograms, which gave mean brightness of 4500, 25 300, and 13 300 CCD counts for Qdot705 and PFS1 and PFS2 Pdots, respectively.

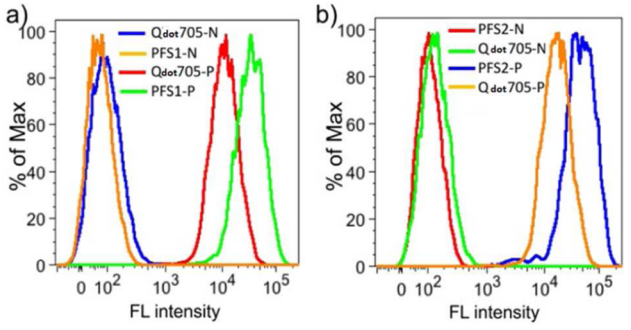

Figure 5. Flow cytometry measurements of the labeling intensity of MCF-7 breast-cancer cells labeled with Qdot705-streptavidin, PFS1 Pdot-streptavidin, and PFS2 Pdot-streptavidin in the presence (positive labeling, P) and absence (negative control, N) of biotinylated primary antibody against the cell-surface protein EpCAM. (a) Comparison between Qdot705 and PFS1 Pdots; fluorescence of labeled cells was collected with a 695/40 nm band-pass filter; excitation at 405 nm. (b) Comparison between Qdot705 and PFS2 Pdots; fluorescence of labeled cells was collected with a 710/20 nm band-pass filter; excitation at 405 nm.

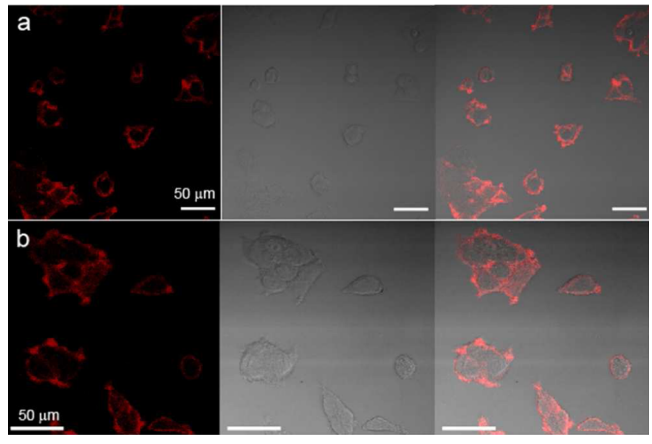

Figure 6. Confocal fluorescence microscopy images of MCF-7 cells labeled with (a) PFS1 Pdot-streptavidin via binding to biotinylated anti-EpCAM primary antibody and (b) PFS2 Pdot-streptavidin via binding to biotinylated anti-EpCAM primary antibody. From left to right: fluorescence images, Nomarski images, and merged fluorescence and Nomarski images; scale bars are 50 μm.

CONCLUSION

In summary, we successfully developed two types of near-infrared-emitting polymer dots with large Stokes shift based on narrow-band emissive squaraine derivatives. Rather than FRET, we believe that efficient exciton diffusion along the fluorene polymer followed by through-bond energy transfer occurred in the PFS Pdots. This mechanism enabled us to develop NIR-emitting Pdots with large Stokes shift, high quantum yield, and narrow emission bandwidth, even in the absence of significant spectral overlap between energy donor and acceptor. Single-particle brightness measurements and flow-cytometry experiments both indicate that the PFS Pdots can be up to 6 times brighter when compared with Qdot705, while the emission bandwidths of the PFS Pdots are about 2 times narrower than that of Qdot705. These superior performance features should make PFS Pdots a valuable new addition in the near-IR region for multiplex biological imaging and analysis.

ASSOCIATED CONTENT

Supporting Information

Materials, experimental details, and supplementary figures and synthetic schemes. This material is available free of charge via the Internet at http://pubs.acs.org.

AUTHOR INFORMATION

Corresponding Author

chiu@chem.washington.edu

dx.doi.org/10.1021/ja5123045 | J. Am. Chem. Soc. 2015, 137, 173−178

Present Address
[‖]Department of Chemistry, National Sun Yat-sen University, 70 Lien Hai Road, Kaohsiung, Taiwan 80424.

Author Contributions
[‡]I-C.W. and J.Y. contributed equally.

Notes
The authors declare the following competing financial interest(s): J.Y., C.W., X.-H.Z., and D.T.C. have financial interest in Lamprogen, which has licensed the described technology from the University of Washington.

■ ACKNOWLEDGMENTS

We gratefully acknowledge support for this research from the National Institutes of Health (R21CA186798) and the University of Washington. C.W. acknowledges financial support from "Thousand Young Talents Program" and the National Science Foundation of China (Grant Nos. 61222508 and 61335001).

■ REFERENCES

(1) Tung, C. H.; Lin, Y. H.; Moon, W. K.; Weissleder, R. *ChemBioChem* **2002**, *3*, 784.
(2) Escobedo, J. O.; Rusin, O.; Lim, S.; Strongin, R. M. *Curr. Opin. Chem. Biol.* **2010**, *14*, 64.
(3) Kovar, J. L.; Simpson, M. A.; Schutz-Geschwender, A.; Olive, D. M. *Anal. Biochem.* **2007**, *367*, 1.
(4) Achilefu, S. *Angew. Chem., Int. Ed.* **2010**, *49*, 9816.
(5) Nesterova, I. V.; Verdree, V. T.; Pakhomov, S.; Strickler, K. L.; Allen, M. W.; Hammer, R. P.; Soper, S. A. *Bioconjugate Chem.* **2007**, *18*, 2159.
(6) Kukrer, B.; Akkaya, E. U. *Tetrahedron Lett.* **1999**, *40*, 9125.
(7) Dilek, G.; Akkaya, E. U. *Tetrahedron Lett.* **2000**, *41*, 3721.
(8) Oswald, B.; Lehmann, F.; Simon, L.; Terpetschnig, E.; Wolfbeis, O. S. *Anal. Biochem.* **2000**, *280*, 272.
(9) Brasseur, N.; Nguyen, T.-L.; Langlois, R.; Ouellet, R.; Marengo, S.; Houde, D.; van Lier, J. E. *J. Med. Chem.* **1994**, *37*, 415.
(10) Chan, W. C. W.; Maxwell, D. J.; Gao, X.; Bailey, R. E.; Han, M.; Nie, S. *Curr. Opin. Biotechnol.* **2002**, *13*, 40.
(11) Zheng, J.; Zhang, C.; Dickson, R. M. *Phys. Rev. Lett.* **2004**, *93*, No. 077402.
(12) Michalet, X.; Pinaud, F. F.; Bentolila, L. A.; Tsay, J. M.; Doose, S.; Li, J. J.; Sundaresan, G.; Wu, A. M.; Gambhir, S. S.; Weiss, S. *Science* **2005**, *307*, 538.
(13) Medintz, I. L.; Uyeda, H. T.; Goldman, E. R.; Mattoussi, H. *Nat. Mater.* **2005**, *4*, 435.
(14) Somers, R. C.; Bawendi, M. G.; Nocera, D. G. *Chem. Soc. Rev.* **2007**, *36*, 579.
(15) Soo Choi, H.; Liu, W.; Misra, P.; Tanaka, E.; Zimmer, J. P.; Itty Ipe, B.; Bawendi, M. G.; Frangioni, J. V. *Nat. Biotechnol.* **2007**, *25*, 6.
(16) Wu, C.; Bull, B.; Szymanski, C.; Christensen, K.; McNeill, J. *ACS Nano* **2008**, *2*, 2415.
(17) Yu, J.; Wu, C.; Sahu, S. P.; Fernando, L. P.; Szymanski, C.; McNeill, J. *J. Am. Chem. Soc.* **2009**, *131*, 18410.
(18) Wu, C.; Schneider, T.; Zeigler, M.; Yu, J.; Schiro, P. G.; Burnham, D. R.; McNeill, J. D.; Chiu, D. T. *J. Am. Chem. Soc.* **2010**, *132*, 15410.
(19) Ye, F. M.; Wu, C. F.; Jin, Y. H.; Chan, Y. H.; Zhang, X. J.; Chiu, D. T. *J. Am. Chem. Soc.* **2011**, *133*, 8146.
(20) Yu, J.; Wu, C.; Zhang, X.; Ye, F.; Gallina, M. E.; Rong, Y.; Wu, I. C.; Sun, W.; Chan, Y.-H.; Chiu, D. T. *Adv. Mater.* **2012**, *24*, 3498.
(21) Rong, Y.; Wu, C.; Yu, J.; Zhang, X.; Ye, F.; Zeigler, M.; Gallina, M. E.; Wu, I. C.; Zhang, Y.; Chan, Y.-H.; Sun, W.; Uvdal, K.; Chiu, D. T. *ACS Nano* **2013**, *7*, 376.
(22) Wu, C. F.; Chiu, D. T. *Angew. Chem., Int. Ed.* **2013**, *52*, 3086.
(23) Jin, Y. H.; Ye, F. M.; Zeigler, M.; Wu, C. F.; Chiu, D. T. *ACS Nano* **2011**, *5*, 1468.
(24) Xiong, L. Q.; Shuhendler, A. J.; Rao, J. H. *Nat. Commun.* **2012**, 3.
(25) Zhang, X.; Yu, J.; Rong, Y.; Ye, F.; Chiu, D. T.; Uvdal, K. *Chem. Sci.* **2013**, *4*, 2143.
(26) Han, M.; Gao, X.; Su, J. Z.; Nie, S. *Nat. Biotechnol.* **2001**, 19.
(27) Lin, W.; Yuan, L.; Cao, Z.; Feng, Y.; Song, J. *Angew. Chem., Int. Ed.* **2010**, *49*, 375.
(28) Jiao, G.-S.; Thoresen, L. H.; Burgess, K. *J. Am. Chem. Soc.* **2003**, *125*, 14668.
(29) Lyons, B. P.; Monkman, A. P. *Phys. Rev. B* **2005**, *71*, 235201.
(30) Bruno, A.; Reynolds, L. X.; Dyer-Smith, C.; Nelson, J.; Haque, S. A. *J. Phys. Chem. C* **2013**, *117*, 19832.
(31) Peckus, D.; Devižis, A.; Hertel, D.; Meerholz, K.; Gulbinas, V. *Chem. Phys.* **2012**, *404*, 42.
(32) Wu, C.; Hansen, S. J.; Hou, Q.; Yu, J.; Zeigler, M.; Jin, Y.; Burnham, D. R.; McNeill, J. D.; Olson, J. M.; Chiu, D. T. *Angew. Chem., Int. Ed.* **2011**, *50*, 3430.
(33) Bharadwaj, P.; Novotny, L. *Nano Lett.* **2011**, *11*, 2137.